Journal of Constructional Steel Research 133 (2017) 84–96

Contents lists available at ScienceDirect

Journal of Constructional Steel Research

Numerical and parametric studies on steel-elastic concrete composite structures

Jia-Bao Yan, Zhong-Xian Li, Jian Xie *

School of Civil Engineering, Tianjin University, Tianjin 300072, China
Key Laboratory of Coast Civil Structure Safety of Ministry of Education, Tianjin University, Ministry of Education, Tianjin 300072, China

ARTICLE INFO

Article history:
Received 27 August 2016
Received in revised form 24 January 2017
Accepted 11 February 2017
Available online xxxx

Keywords:
Steel-concrete composite structure
Finite element analysis
Push-out test
Numerical analysis
Steel-concrete composite beam
Three-dimensional analysis

ABSTRACT

This paper provided an overview on the developments of the steel-elastic concrete composite (SECC) structures. 16 push-out tests and six beam tests were reported to demonstrate the ultimate strength behaviour of the SECC structure from the component level to the structure level. Three-dimensional finite element models (FEMs) have been developed to simulate the ultimate strength behaviour of the SECC structures. The developed FEMs considered the nonlinear mechanical properties of the elastic concrete and steels in the structure, geometric nonlinearities, and complex interactions among the headed studs, I-beam, and concrete slabs. Extensive validations of the numerical analyses against the reported 16 push-out tests and six beam tests proved that the developed FEMs offered reasonable simulations on the ultimate strength behaviour of the SECC structure from component level to the structural level in terms of ultimate resistances, load-slip (or deflection) behaviours, and failure modes. A subsequent parametric study was carried out to investigate the influences of the rubber content in the elastic concrete and strength of the I-beam on the ultimate strength behaviour of the SECC beams. Finally, step-by-step FE analysis procedures on the SECC structures were recommended based on these numerical studies and validations.

1. Introduction

Elastic concrete, i.e., concrete with addition of tire rubber, exhibits improvements on its crack and fatigue resistance. The added rubber particles in elastic concrete were usually recycled from the crushed waste rubber (e.g., automobile tires) that could reduce the environmental pollution, result in green constructions, and reduce carbon dioxide emission. The elastic concrete was initially developed for the road pavement in 1990s [1]. Pilot research by Eldin and Senouci [2] showed that the concrete with tire chips and crumb rubber exhibited lower strength but more ductile behaviour under compression than that of concrete without rubber. Continued works by Topcu and Toutanji [3,4] also proved that the elastic concrete with tire rubber improved its toughness [3,4]. Further tests [5,6] also showed that elastic concrete with crushed rubbers exhibited reductions in the flexural tensile strength, but increased its fracture strain. The three-point bending tests under fatigue loading by Feng et al. [7] proved that the fatigue resistance of the elastic concrete was significantly improved. Including the improved fracture toughness, deformability and fatigue resistance, the elastic concrete also exhibits advantages of superior acoustical behaviours, aging and wearing resistance over conventional normal weight concrete. This type of relative new material has been extensively used as the pavements for roads and bridges, parking lots, and sport court. More recently, it has been used in the steel-concrete composite structures, i.e., steel-elastic concrete composite (SECC) structures.

SECC structure typically consists of a concrete slab connected to the underneath I-beams through the cohesive materials (e.g., epoxy) or headed shear studs. This type of structure combines the advantages of concrete compression and steel tension, and has been widely used in the residential and commercial buildings, bridges, and multi-story factories. In steel-concrete composite structures, the strengths of the concrete and shear connectors are important to the ultimate load carrying capacity of the structure. Kim et al. [8] experimentally studied the influence of the degree of the composite action on the ultimate loading carrying capacity of the steel-concrete composite beam, and found that this influence was quite limited. Experiments carried out by Nie et al. [9] also showed that partial composite steel-concrete composite beams could also be used in the continuous steel-composite beams if proper measures were taken. More recently, the steel-concrete composite beam with elastic concrete has been developed for engineering constructions [10–13]. Preliminary experimental studies showed that using the elastic

Abbreviations: CDM, continuum damage model; CDP, concrete damage plasticity; COV, coefficient of variation; FE, finite element; FEA, finite element analysis; FEM, finite element model; HSS, headed shear stud connector; SECC, steel-elastic concrete composite structure.

* Corresponding author at: School of Civil Engineering, Tianjin University, Tianjin 300072, China.
E-mail address: xiejian@tju.edu.cn (J. Xie).

http://dx.doi.org/10.1016/j.jcsr.2017.02.010
0143-974X/

Nomenclature

D_c, D_t	compressive and tensile damage ratios of concrete, respectively
E_0	initial elastic modulus of concrete
E_s	elastic modulus of the steel
H	height of the I-beam in the SECC composite beam
K_e	experimental elastic stiffness in the load-central deflection curves of the SECC beam
$K_{e,FE}$	numerical elastic stiffness in the load-central deflection curves of the SECC beam
P	resistance of the SECC composite beam
$P_{u,FE}$	ultimate resistance of SECC structure predicted by the finite element analysis
$P_{u,t}$	experimental ultimate resistance of SECC structure
S_1, S_2	spacing of the connectors in mid-span and side span as shown in Fig. 3
T	thickness of the concrete slab as shown in Fig. 3
W	width of the I-beam as shown in Fig. 3
a	with of the flange of the concrete slab as shown in Fig. 3
f_c	compressive stress at the softening region in the stress-strain curve
f_{ck}	compressive stress at the softening region in the stress-strain curve
f_{yr}, f_{ur}	yield and ultimate strength of the reinforcement in the concrete slab
f_{yl}, f_{ul}	yield and ultimate strength of the I-beam
n_s	quantity of the headed studs in half span of the SECC beams
δ_f	central deflection of the steel-elastic concrete composite beam
ε_c	compressive strain of the concrete
ε_{ck}	compressive strain of the concrete corresponding to f_{ck}
ε_c^{In}, ε_t^{In}	inelastic compressive or tensile strain of the concrete
$\bar{\varepsilon}_c^{In}$, $\bar{\varepsilon}_t^{In}$	inelastic compressive and tensile strain against the maximum strain in the stress-strain curves
ε_c^{pl}, ε_t^{pl}	true compressive or tensile plastic strain of the concrete
ρ	rubber content by volume of the elastic concrete
σ_c, σ_t	uniaxial tensile compressive or tensile stress of concrete
σ_y, σ_u	yield and ultimate strength of the headed studs
Δ	interfacial slip between the I-beam and concrete slab in the push-out test
υ	Poisson's ratio

concrete improved the fatigue resistance of the steel-concrete composite beams, which becomes more essential to the bridges with steel-concrete composite decks.

Since the SECC structures have been developed for civil constructions, their structural behaviours need to be well understood. Push-out tests were widely carried out to obtain the shear-slip behaviour of the headed shear studs in steel-concrete composite structures. Extensive experimental works on shear strength behaviour of the headed studs in different normal and lightweight concrete have been reported by Viest et al. [14], Ollgaard et al. [15], Lam et al. [16], and Tahir et al. [17]. Yan et al. [18] have reported 102 push-out tests on specimens with J-hook types of connectors. Xie et al. [19] reported 24 push-out tests on laser welded bar connectors used in the Bi-steel type of steel-concrete composite structure. However, these experimental studies focused on the shear strength behaviour of the connectors mainly embedded in normal- or light-weight concrete. The information on the shear strength of stud connectors in elastic concrete is still quite limited. In addition, specifications on shear strength of the headed studs in most of the design codes, e.g., Eurocode 4 and ANSI/AISC, are empirical that were developed through regression analysis on the push-out tests. Thus, the design recommendations in Eurocode 4 and ANSI/AISC need to be checked on the predictions on shear resistance of connectors in steel-elastic concrete composite structure. From this point of view, the push-out tests on headed studs embedded in elastic concrete are still required and of importance to the development of design equations on the strength of the SECC structures.

The full scale tests on strength behaviour of the headed studs and beams tend to be costing and could not offer the thorough understanding on the structural behaviour of the SECC structures. Finite element (FE) simulation usually offers the alternative to analyse the structural behaviours of the steel-concrete composite structures. FE models that detailed simulate the connectors in push-out tests have been reported by Nguyen et al. [20], Pavlović et al. [21], Lam and Ellobody [22], Guezouli et al. [23], and Yan et al. [24]. However, it was found that the detailed simulation on the headed stud connectors as well as on the concrete surrounding the connectors would lead to a large quantity of element in FE modelling (FEM). Therefore, simplifications of the headed stud in the steel-concrete composite structures become popular in the last two decades. Spring element or cohesive material was used in the FEM instead of connectors through assigning experimental shear-slip behaviours to the spring or cohesive materials [24–27]. Zhao and Li [25] developed a 3D FE model for the steel-concrete composite beam by simplifying the shear connectors with cohesive material. Song et al. [26] used spring element to simulate the headed studs used in the steel-concrete composite structures under fire hazard. Though this simplified method could efficiently improve the computing efficiency, the spring element used in the FEM just adopted the shear-slip behaviour of the stud from the push-out tests. However, previous studies showed that the shear and tensile resistance of the stud connector would compensate each other, and this shear-tension interaction strength of the headed stud connectors could not be precisely simulated that would compromise the accuracy of the FE simulation [27]. Thus, it is necessary to develop a FEM with detailed simulation of the headed stud connectors for the steel-concrete composite structure, especially for SECC beams.

This paper aimed to develop the three-dimensional nonlinear finite element model (FEM) for SECC beams. Firstly, the paper briefly introduced the developments of steel-elastic concrete composite beams. The push-out tests and four-point bending tests on the SECC beams [10–13] were then introduced that were used to experimentally study the structural behaviour of SECC structure on the component level to the structural level, respectively. Then, the FEMs were developed for the push-out tests and SECC beams in four-point bending tests. The accuracies of these developed FEMs were validated against these reported push-out and beam tests. Parametric studies were also carried out to investigate the influences of the rubber content and steel strength of the I-beam on ultimate strength behaviour of SECC beams. Finally, FE analysis procedures for the SECC structures were recommended.

2. Experimental studies on the steel-elastic concrete composite structure

Sixteen push-out tests and six quasi-static tests were carried out on component specimens with headed studs and SECC beams, respectively. Elastic concrete with different volume fraction of crumb rubber were used in all the 24 specimens.

2.1. Materials

The elastic concrete used in this test program consists of ordinary Portland cement (P.O. 42.5) [see Fig. 1(a)], water, granite coarse aggregate [see Fig. 1(b)], fine aggregate [natural sand, see Fig. 1(c)], and rubber particles as shown in Fig. 1(d). The crushed granite stone type of coarse aggregate with particle diameter of 5– 25 mm was used in the mixture. The maximum particle diameter and fineness modulus for

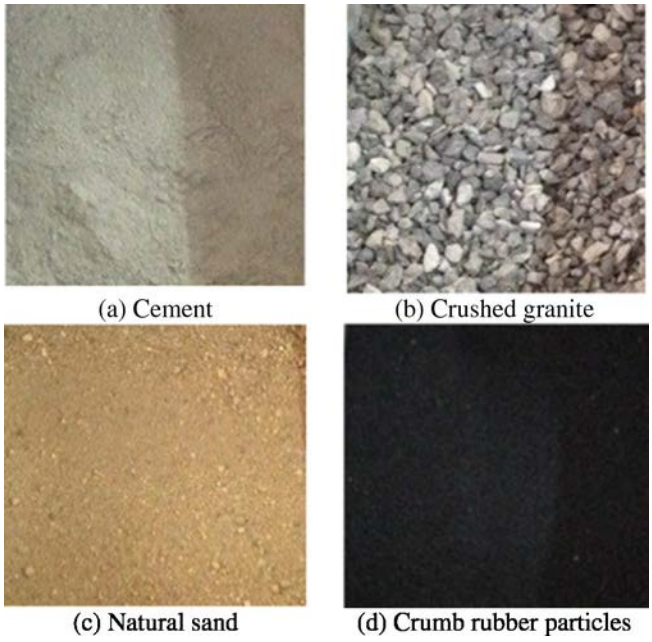

Fig. 1. Raw materials in elastic concrete.

the natural sand type of fine aggregate used in the mixture were 5 mm and 0.22, respectively. Different volume fractions of the crumb rubber were used in the concrete to investigate their influences on the structural behaviours of the steel-elastic concrete composite structure. The different volume fractions of crumb rubber used in the push-out tests were 0%, 5% (50 kg/m^3), 10% (100 kg/m^3), and 15% (150 kg/m^3) whilst only two types of volume fractions, i.e., 0% and 10% (100 kg/m^3) were used in the beam tests. Table 1 lists the mixture proportions of all the concretes involved in this test program. For each kind of concrete mixture, three concrete cubes (150 × 150 × 150 mm^3) and prisms (100 × 100 × 300 mm^3) were prepared together with the specimens and cured in the standard environment. Following the testing methods in GB/TB50081-2002 [28] and T0555-2005 [29], the mechanical proportions of all the elastic concretes involved in this test program are listed in Table 2.

Nelson studs, i.e., headed stud connectors, were used in the push-out and beam tests. The Ø16 mm and Ø19 mm headed studs were used in push-out tests, and Ø16 mm, Ø19 mm, and Ø22 mm headed studs were used in the steel-elastic concrete composite beam specimens. More details of the headed studs are shown in Fig. 1. The mechanical properties of the studs were obtained from the tensile tests according to ASTM A370-13 [30] as listed in Table 2 and depicted in Fig. 2.

2.2. Push-out tests [31]

Sixteen specimens for push-out tests were prepared, and they were categorized into six groups with two or three identical specimens in each group [31]. The parameters studied in this test program were volume fraction of the fiber content, strength of the elastic concrete, and diameter of the headed stud connectors. Fig. 2(a) shows the typical specimen used for the push-out test that consists of I-beam, headed stud connectors, reinforcement mesh, and concrete slab. HW200 × 200 × 12 × 8 type of I-beam was chosen for each specimen, and its yield and ultimate strength are 235 MPa and 400 MPa, respectively. The concrete slab measures 460 mm, 400 mm, and 160 mm in length, width, and depth, respectively. Grade 4.6 type of headed studs was used in the push-out specimens with the yield and ultimate strength of 240 MPa and 400 MPa, respectively. The geometric details of the headed studs were listed in Table 2 and depicted in Fig. 2(b). Ø10 mm reinforcement mesh with yield strength of 335 MPa was used in the concrete slabs. Table 2 lists the details of all the specimens for the push-out tests. The interfacial slip between the concrete slabs and I-beam was measured by the linear varying displacement transducers (LVDTs) during each test. More details of these push-out tests were reported by Han et al. [31].

Table 1
Mix proportions of different elastic concretes (kg/m^3).

Type	Rubber	Water	OPC	CA	FA	SP ADVA181
EC-C30-0%	0	165	295	1087	839	2.17
EC-C30-5%	50	169	400	703	1004	2.39
EC-C30-10%	100	168	590	1230	412	6.52
EC-C30-15%	150	168	590	1230	412	7.39
EC-C40-5%	50	169	550	703	1004	5.65

EC-C30-0% denotes elastic concrete-Grade 30-0% volume fraction of rubber; OPC denotes ordinary Portland cement; CA denotes granite type of coarse aggregate; FA denotes natural sand type of fine aggregate; SP denotes the superplasticizer.

2.3. Steel-elastic concrete composite beams under two-point loading

Six specimens in total namely B1–6 were prepared for the quasi-static tests under two-point loading [11]. All the specimens were 4000 mm long and simply supported with a clear span of 3700 mm as shown in Fig. 3. The distance between the two loading points was 700 mm. As shown in Fig. 3, the cross section of the six specimens were 600 mm in width, but designed with varying depths for different specimens. Two types of I-beams, i.e., HW250 × 250 and HW300 × 300, were used to fabricate the composite beams, and details of these two types of sections are depicted in Fig. 3 and given in Table 3. Stiffeners were installed on the I-beams at the locations underneath the loading point and at the supports to enhance its local shear resistances and prevent shear failure. The parameters studied in this test program were volume fraction of the rubber, depth of the concrete slab, diameter of the headed studs, and composite degree of the beam (i.e., spacing of the headed stud connectors). Two different volume fractions of the rubber (i.e., 0% and 10%) were used in the steel-elastic concrete composite beams B1 (or B4) and B2 (or B5), respectively. B2 and B3 were designed with the same geometry and materials but different spacing of headed studs of 140 mm and 100 mm, respectively. Finally, B5 and B6 were designed with the same composite action of the section but with headed studs in different diameter. The mid-span deflection, end relative slip between the concrete slab and I-beam, and uplifting of the concrete slabs were measured by the linear varying displacement transducers (LVDTs). Table 3 and Fig. 3 offer more details of these six specimens.

3. Finite element modelling

3.1. General

General commercial FE code ABAQUS was used for the FE modelling of the push-out tests and beams tests on specimens with elastic concrete [32]. Considering the material and geometric nonlinearities in the FE simulation, ABAQUS/Explicit type of solver was used in the FE analysis to overcome the convergence problem.

3.2. Modelling of elastic concrete

Concrete damage plasticity (CDP) model in ABAQUS material library [31] was chosen for the elastic concrete materials involved in this study. According to the ABAQUS user manual [32], the CDP model adopts the isotropic plasticity for both tension and compression with isotropic damage to simulate the inelastic behaviours of concretes [32]. The yield function proposed by Lee and Fenves [33] was used to describe the evolution of strength of concrete under both compression and tension. The CDP model also followed the isotropic damage and non-

Table 2
Material and geometric details and test results of the push-out tests.

Specimen	ρ (%)	f_{ck} (MPa)	$d \times h$ (mm^2)	Reinforcement		f_{yr} (MPa)	f_{ur} (MPa)	$f_{y,l}$ (MPa)	$f_{u,l}$ (MPa)	σ_y (MPa)	σ_u (MPa)	$P_{u,t}$ (kN)	$P_{u,FE}$ (kN)	$\frac{P_{u,t}}{P_{u,FE}}$
				Horizontal	Vertical									
P1	0	34.1	16 × 90	Φ10@95	Φ10@110	335	445	235	400	240	400	156	163.3	0.96
P2	0	34.1	16 × 91	Φ10@95	Φ10@110	335	445	235	400	240	400	158.7	163.3	0.97
P3	0	34.1	16 × 92	Φ10@95	Φ10@110	335	445	235	400	240	400	163.3	163.3	1.00
P4	5	26.8	16 × 90	Φ10@95	Φ10@110	335	445	235	400	240	400	163.8	153.7	1.07
P5	5	26.8	16 × 90	Φ10@95	Φ10@110	335	445	235	400	240	400	153.5	153.7	1.00
P6	5	26.8	16 × 90	Φ10@95	Φ10@110	335	445	235	400	240	400	153.4	153.7	1.00
P7	10	34.1	16 × 90	Φ10@ 95	Φ10@110	335	445	235	400	240	400	149.7	157.2	0.95
P8	10	34.1	16 × 90	Φ10@ 95	Φ10@110	335	445	235	400	240	400	133.8	157.2	0.85
P9	10	34.1	16 × 90	Φ10@ 95	Φ10@110	335	445	235	400	240	400	150.4	157.2	0.96
P10	15	29.4	16 × 90	Φ10@95	Φ10@110	335	445	235	400	240	400	139.2	145.5	0.96
P11	15	29.4	16 × 90	Φ10@95	Φ10@110	335	445	235	400	240	400	119.3	145.5	0.82
P12	5	37.8	16 × 90	Φ10@95	Φ10@110	335	445	235	400	240	400	159.5	147.2	1.08
P13	5	37.8	16 × 90	Φ10@95	Φ10@110	335	445	235	400	240	400	156.5	147.2	1.06
P14	5	26.8	19 × 110	Φ10@95	Φ10@110	335	445	235	400	240	400	220.0	204.4	1.08
P15	5	26.8	19 × 110	Φ10@95	Φ10@110	335	445	235	400	240	400	193.3	204.4	0.95
P16	5	26.8	19 × 110	Φ10@95	Φ10@110	335	445	235	400	240	400	205.3	204.4	1.00
Mean														0.98
Stdev														0.07

ρ denotes volume fraction of the rubber in concrete; $d \times h$ denotes diameter by height of the stud connectors; f_{ck} denotes compressive strength of concrete; f_{yr}, f_{ur} denote yield and ultimate strength of reinforcement mesh, respectively; σ_y, σ_y denote yield and ultimate strength of the headed studs, respectively; $P_{u,t}$, $P_{u,FE}$ denote experimental and numerical ultimate shear resistance of push-out test specimen.

associated potential flow rule as specified in ABAQUS [27]. In CDP model, uniaxial tensile and compressive behaviours were described by the plastic stress-strain curves and damage parameters. There are mainly two ways to define the compressive or tensile stress-strain curves of the elastic concrete involved in this study. The first way could adopt the experimental stress-strain curves, and the second way may adopt the concrete model introduced by Carreira and Chu [34] as the following;

$$f_c = \frac{f_{ck}\beta(\varepsilon_c/\varepsilon_{ck})}{\left[\beta - 1 + (\varepsilon_c/\varepsilon_{ck})^{\beta}\right]} \tag{1}$$

$$\beta = (f_{ck}/32.4) + 1.55 \tag{2}$$

where, f_c and ε_c denote the compressive stress and strain of the concrete, respectively; f_{ck} denotes the characteristic uniaxial compressive strength of the concrete; and ε_c denotes the strain corresponding to f_{ck}.

Zhu et al. [35] have reported a series of tests on compressive and flexural tensile stress-strain curves of the elastic concrete with different volume fraction of the rubber as shown in Fig. 4(a) and (b). The compressive stress-strain curves of the elastic concrete with different rubber content were also reported by Han et al. [31] and Xing et al. [11] as shown in Fig. 4(c) and (d). All these presented stress-strain curves as shown Fig. 4(a)–(d) could be used as the input stress-strain curves in CDP model. In ABAQUS material library, these obtained uniaxial tensile and compressive engineering stress-strain curves need to be converted to the stress versus inelastic strain curves as the input data [27]. The CDP model also needs to specify the damage parameters to describe the strain softening. The compressive or tensile damage parameters D_c(orD_t) versus inelastic strain ε_c^{In}(orε_t^{In}) curves can be defined as follows [27]

$$\varepsilon_c^{pl} = \varepsilon_c^{In} - \frac{D_c}{(1-D_c)}\frac{\sigma_c}{E_0} \tag{3}$$

$$\varepsilon_t^{pl} = \varepsilon_t^{In} - \frac{D_t}{(1-D_t)}\frac{\sigma_t}{E_0} \tag{4}$$

where, ε_t^{pl} and ε_c^{pl} denote true tensile or compressive plastic strain of the concrete, respectively; ε_t^{In} and ε_c^{In} denote inelastic tensile or compressive strain of the concrete, respectively; D_c and D_t denote the compressive and tensile damage ratio, respectively.

The D_c(orD_t) can be determined according to the proposed functions by Wang et al. [36] as the follows

$$D_c = A_c e^{-\bar{\varepsilon}_c^{In}/t_c} + B_c \tag{5}$$

$$D_t = A_t e^{-\bar{\varepsilon}_t^{In}/t_t} + B_t \tag{6}$$

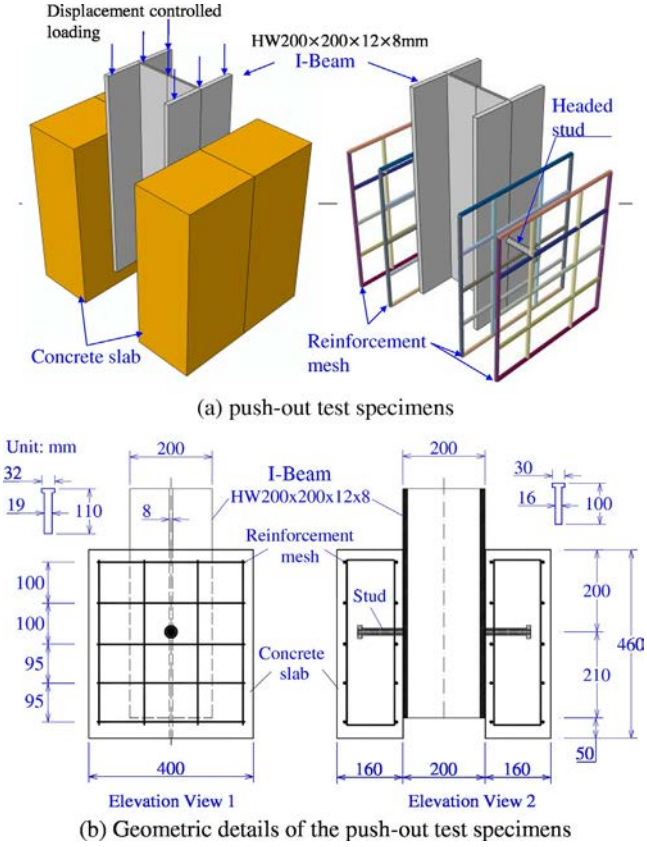

Fig. 2. Details of push-out test specimens.

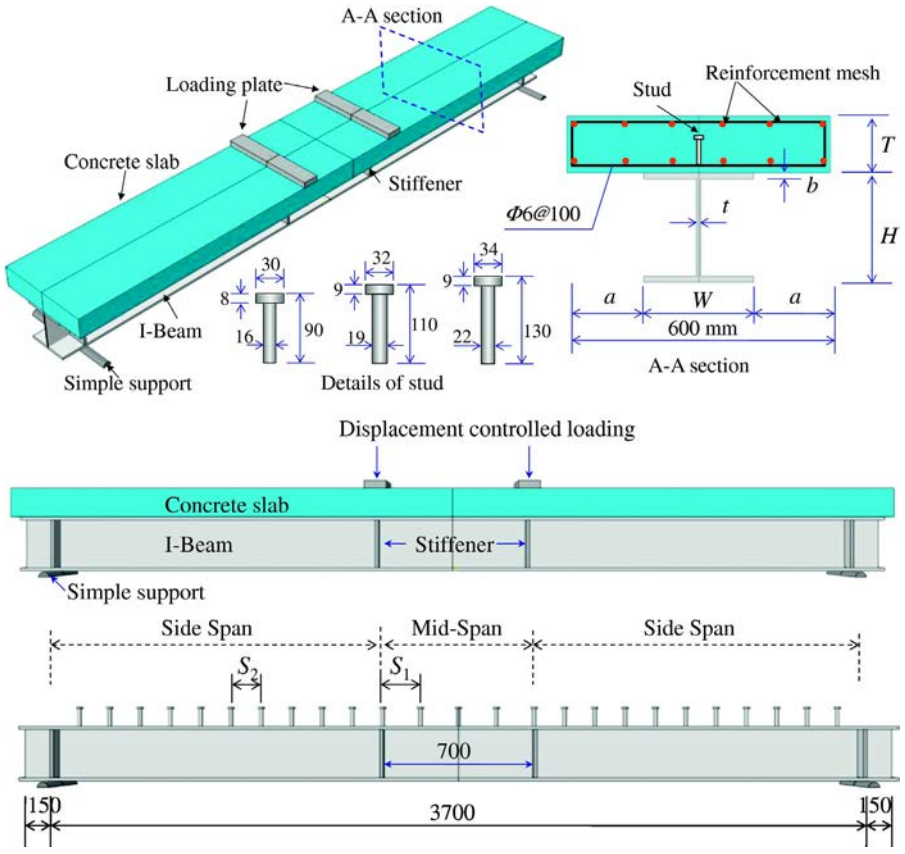

Fig. 3. Details and test setup of steel-elastic concrete composite beams.

where $\overline{\varepsilon}_c^{In}$ and $\overline{\varepsilon}_t^{In}$ refer to the inelastic compressive and tensile strain against the maximum strain in the stress-strain curves, respectively; t_c and t_t are a constant empirical values; $A_c = \frac{1}{e^{-1/t_c}-1}$; $B_c = -\frac{1}{e^{-1/t_c}-1}$; $A_t = \frac{1}{e^{-1/t_t}-1}$; $B_t = -\frac{1}{e^{-1/t_t}-1}$.

The other plasticity parameters in the CDP model of the elastic concrete for flow potential eccentricity, the dilation angels, and ratio of the biaxial/uniaxial compressive strength were 0.1, 23°, and 1.16, respectively.

3.3. Modelling of steel I-beams, studs, and reinforcements

This paper adopted the nonlinear isotropic/kinematic hardening model for the steel materials involved in the experimental studies. This material model adopted the Mises yield surface to define the isotropic yielding of the steel in ABAQUS material library. The typical Bi-linear stress-strain curves for the I-beams and reinforcements were used to define the input stress-strain curves in the material model. Tables 2 and 3 list the mechanical properties of the elastic modulus, Poisson's

Table 3
Material and geometric details and test results of the steel-elastic concrete beams.

Beam	Section type	T (mm)	$W = H$ (mm)	a (mm)	b (mm)	t (mm)	ρ (%)	d (mm)	$S1$ (mm)	$S2$ (mm)	Degree of composite action	f_c (MPa)	E_c (GPa)
CB1	HW250 × 250	130	250	175	14	9	0	16	175	140	0.5	44.3	33.7
CB2	HW250 × 250	130	250	175	14	9	10	16	175	140	0.5	42.5	28.7
CB3	HW250 × 250	130	250	175	14	9	10	16	175	100	0.68	42.5	28.7
CB4	HW300 × 300	160	300	150	19	12	0	19	175	140	0.5	44.3	33.7
CB5	HW300 × 300	160	300	150	19	12	10	19	175	140	0.5	42.5	28.7
CB6	HW300 × 300	160	300	150	19	12	10	22	350	200	0.5	42.5	28.7

Beam	f_{yr} (MPa)	f_{ur} (MPa)	$f_{y,I}$ (MPa)	$f_{u,I}$ (MPa)	σ_y (MPa)	σ_u (MPa)	K_e (kN/mm)	P_u (kN)	Failure mode	$K_{e,FE}$ (kN/mm)	$K_e/K_{e,FE}$	$P_{u,FE}$ (kN)	$P_u/P_{u,FE}$
CB1	388	455	267	402	243	365	33.7	540	FM	37.8	0.89	525	1.03
CB2	388	455	267	402	243	365	30.9	534	FM	34.4	0.90	519	1.03
CB3	388	455	267	402	243	365	34.1	532	FM	36.1	0.94	524	1.02
CB4	388	455	267	402	243	365	108.8	1274	FM	106.3	1.02	1284	0.99
CB5	388	455	267	402	243	365	112.5	1305	FM	105.2	1.07	1276	1.02
CB6	388	455	267	402	243	365	98.3	1158	FM	88.1	1.12	1232	0.94
Mean											0.99		1.01
Stdev											0.09		0.03

T, W, H, a, b, t, $S1$, $S2$ were as shown in Fig. 3; ρ denotes volume fraction of the rubber in concrete; d denotes diameter of the stud connectors; f_c, E_c denote compressive strength and elastic modulus of concrete, respectively; f_{yr}, f_{ur} denote yield and ultimate strength of reinforcement mesh, respectively; σ_y, σ_y denote yield and ultimate strength of the headed studs, respectively; K_e, P_u denote elastic stiffness and ultimate resistance of steel-elastic concrete beam, respectively; $K_{e,FE}$, $P_{u,FE}$ denote elastic stiffness and ultimate resistance of steel-elastic concrete beam predicted by the FEA, respectively.

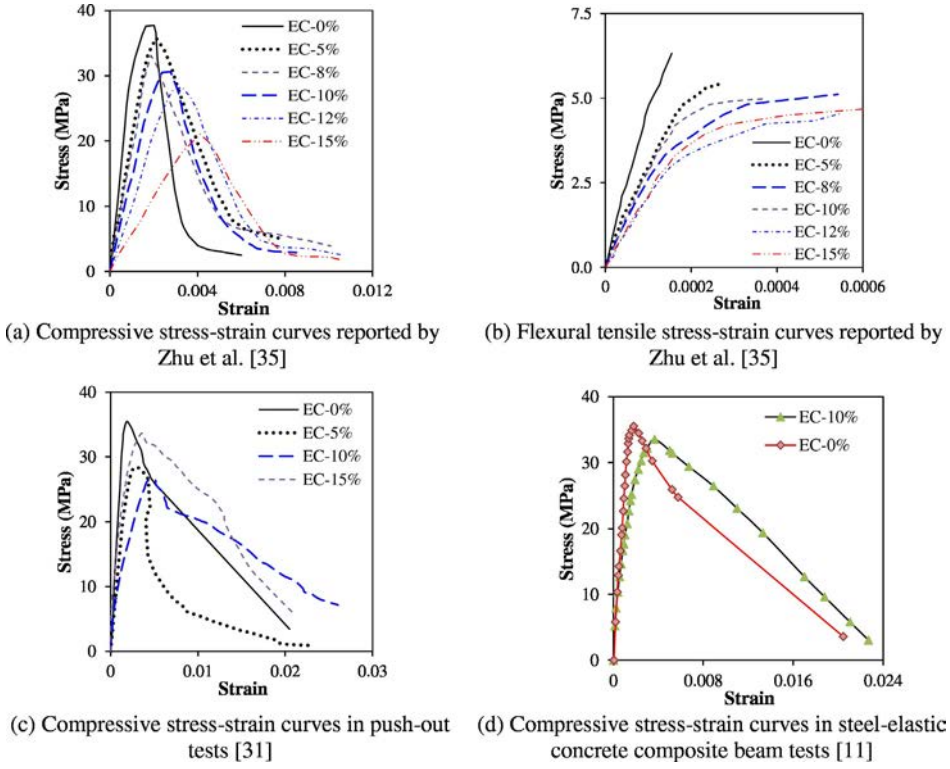

Fig. 4. Experimental uniaxial stress-strain curves of the elastic concrete.

ratio, yield and ultimate strength of the I-beam, reinforcement and headed studs that were obtained from the tensile tests on the steel coupons. Fig. 5(a) shows the bi-linear stress-strain model used in the developed FEM, and Fig. 5(b) shows the representative experimental tensile stress-strain curves.

3.4. Geometry, element types, and mesh size in finite element model

3.4.1. Finite element model for push-out tests

Fig. 6 plots the FEM for the push-out tests. Due to the symmetry of the geometry and loading patterns of the push-out tests, only one fourth of the full geometry was built in the FEM. Different components in the push-out tests were modelled that included concrete slabs, reinforcement mesh, I-Beam, and testing base. The headed studs in the FEM were detailed simulated with the same geometry as those used in the push-out tests, and concrete elements at the corresponding positions in the slabs were removed. Three-dimensional eight-node continuum elements (C3D8R) with one integration point were used to model the I-beams, concrete slabs, and headed studs. Two-node three-dimensional truss element-T3D2 was used for the reinforcements in the concrete slab. The truss element shares the same node with the adjacent 3D continuum element. To improve the computing efficiency and accuracy, varying mesh sizes technique was used in this FEM. The mesh sizes for the I-beam were about $8 \times 8 \times 4$ mm^3 in the web, and $8 \times 8 \times 6$ mm^3 in the flange. The mesh size for headed studs was about $4 \times 4 \times 4$ mm^3. The mesh sizes for the elements of the concrete slab near and far away from the headed studs were about $8 \times 8 \times 4$ mm^3 and $8 \times 8 \times 8$ mm^3, respectively.

3.4.2. Finite element model for steel-elastic concrete composite beams

Fig. 7 plots the FEM for the steel-elastic concrete composite beams. One fourth model was also built considering the symmetry of the geometry and loading patterns. The main components including I-beam, headed studs, concrete slabs, reinforcement mesh, loading plate, and

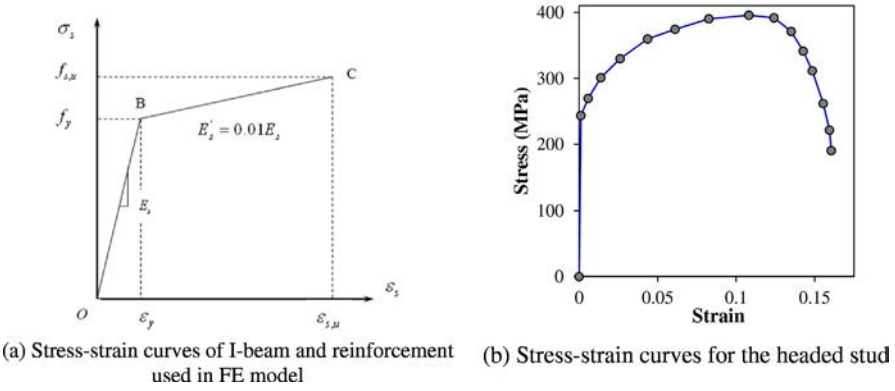

Fig. 5. Stress-strain curves for steel materials involved in the FE model.

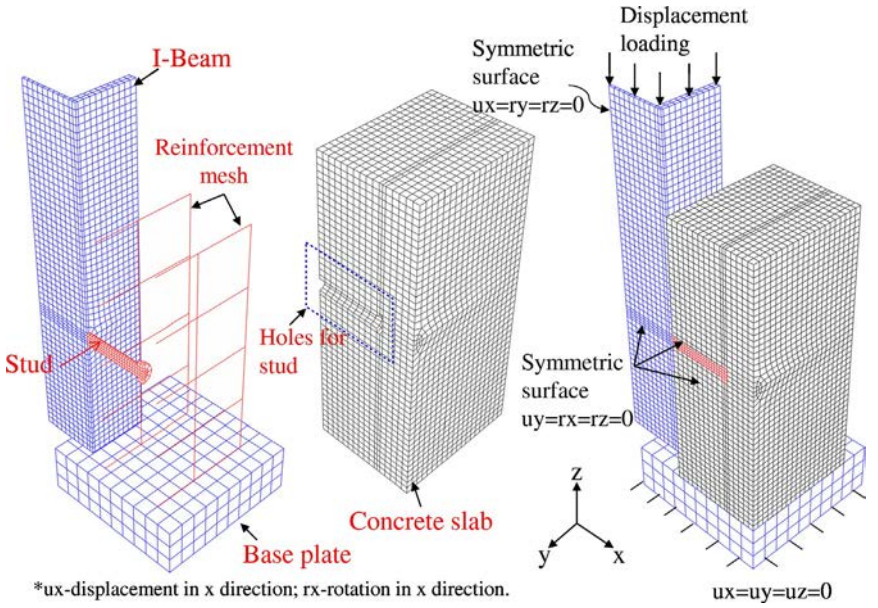

Fig. 6. FE model for push-out test specimen on headed studs in elastic concrete.

support were built in the developed FEM as shown in Fig. 7(b)–(d). In order to properly simulate the essential component (i.e., headed studs) in the composite beams, detailed geometry of the headed studs were built in the FEM. The holes in the concrete slabs for the headed studs were reserved as shown in Fig. 7(e). C3D8R element was used for the modelling of the I-beam, concrete slab, loading plate, support, and headed studs whilst T3D2 was used for the reinforcements in the concrete slab. Different mesh sizes were also used at different locations in the FEM. The mesh size for headed studs were about $4 \times 4 \times 4$ mm^3. The mesh sizes for the elements of the concrete slab near and far away from the headed studs were about $8 \times 8 \times 4$ mm^3 and $8 \times 8 \times 8$ mm^3, respectively whilst the mesh sizes for the I-beam were about

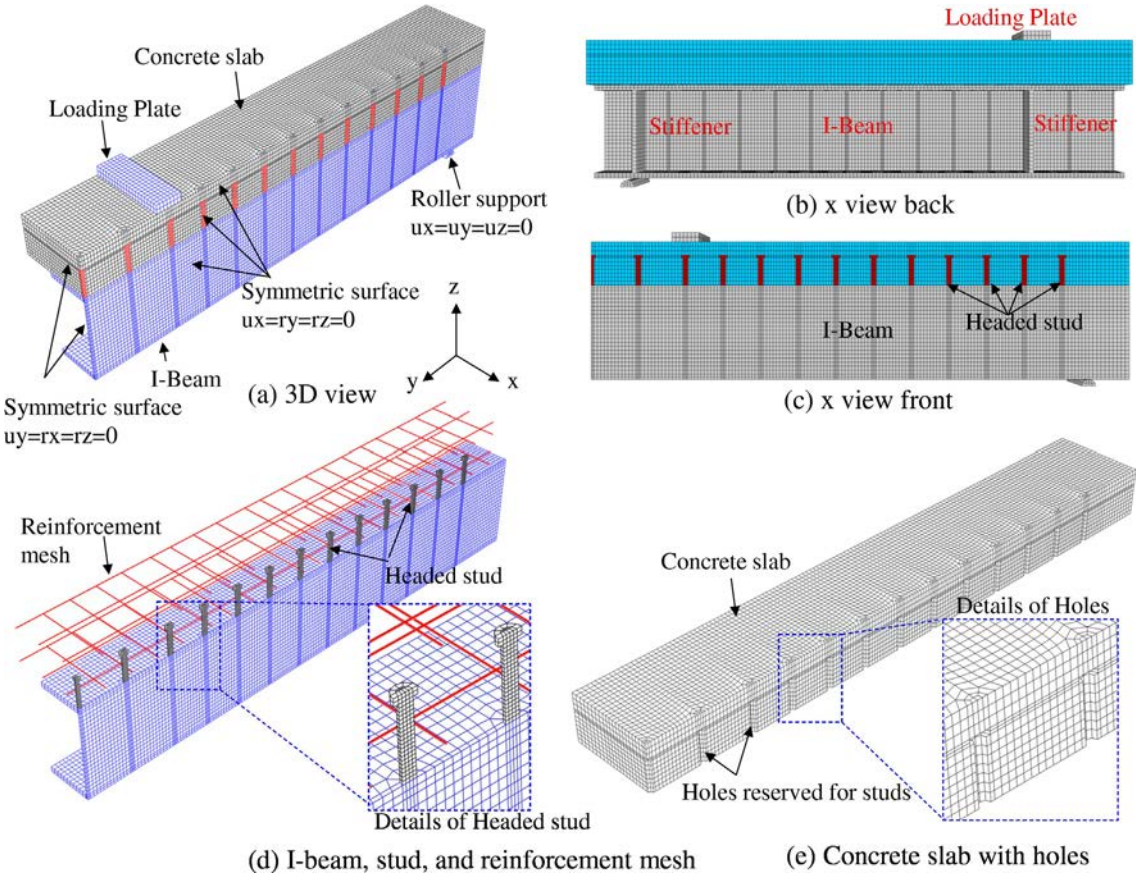

Fig. 7. FE model for steel-elastic concrete composite beam.

$8 \times 8 \times 5$ mm^3 and $8 \times 8 \times 8$ mm^3 for the web and flange, respectively. For the reinforcement, the mesh size is 8 mm.

3.5. Loadings and steel-concrete interactions

Downward displacement type of loadings was applied to the I-beam for the push-out tests (see Fig. 6) and loading plate for the beam tests (see Fig. 7), respectively. In the FEM for the push-out tests, symmetric restraints were applied to two symmetric surfaces as illustrated in Fig. 6. Take the middle surface ZX plane as shown in Fig. 6 for example, the symmetric restraint of uy = 0 (displacement in y direction equals zero) and rx = rz = 0 (rotations along x and z directions equal zero) were applied. For the FEM of steel-elastic concrete beams, there were two symmetric surfaces, i.e., ZY plane and ZX plate at the mid-span, in the FEM as shown in Fig. 7. Symmetric restraints were applied to these two planes as shown in Fig. 7. The roller support was restrained from any movement in three translational degrees of freedom.

Surface-to-surface contact was used to describe the interactions among different components in the push-out tests and beam tests, which include interactions between the headed studs and concrete, interactions between the concrete slabs and I-beam, the concrete slab-base plate interactions in push-out tests, support-I beam interaction (beam tests), and interactions between the loading plate and concrete slab. The master surface in the definition of the interacting pairs chose the relative harder materials, e.g., I-beam, connectors, support whilst the slave surface select the relative softer materials, e.g., the concrete. The contact interacting algorithm allows the penetration of the master surface into the slave surface, but not the vice versa. The normal and tangential interaction behaviours between the master surface and slave surface adopted the "hard contact" algorithm and "penalty friction" algorithm, respectively. In ABAQUS interaction library, the hard contact algorithm permits the transfer of the contact pressure if the two interacting surfaces touch and transfers zero pressure since they are separated. The penalty friction algorithm could simulate different degree of friction forces between the master and slave surfaces through using different values of the friction coefficient. This paper adopted the friction coefficients of 0.25 and 0.3 for the steel-concrete friction and steel-steel friction, respectively.

4. Validations of the finite element model

The FE models developed in this paper were validated by the 16 push-out tests performed by Han et al. [31] and six beam tests carried out by Xing et al. [11].

4.1. Validations of the FE model against push-out tests

Fig. 8(a)–(f) compares the load-slip curves of the 16 push-out tests with those curves that were obtained from the FE analyses. These figures show that the FE model predicted well the load-slip curves of the push-out tests in terms of stiffness, ultimate resistance, and ductility of the headed stud connectors. However, these figures also show that some differences still exist in the load-slip curves between the FE predictions and tests due to the variations of the strength of the elastic concretes and steel materials.

Fig. 9(a) and (b) compares the FE predicted shank shear failure in the headed studs with those experimental observations. It can be found that the developed FE model could capture the shear failure of the headed studs in the elastic concrete.

Table 2 compares all the FE predicted ultimate shear resistances of the headed studs in elastic concrete with those experimental values. The test-to-prediction ratio was used to evaluate the accuracy of the FE predictions. From Table 2, it can be found that the average test-to-prediction ratio for 16 push-out tests was 0.98 with a standard deviation (Stdev) of 7%. The above validations confirmed that the developed FE model could simulate well the ultimate strength behaviour of the basic component of the steel-elastic concrete composite structures, i.e., the headed shear stud in elastic concrete.

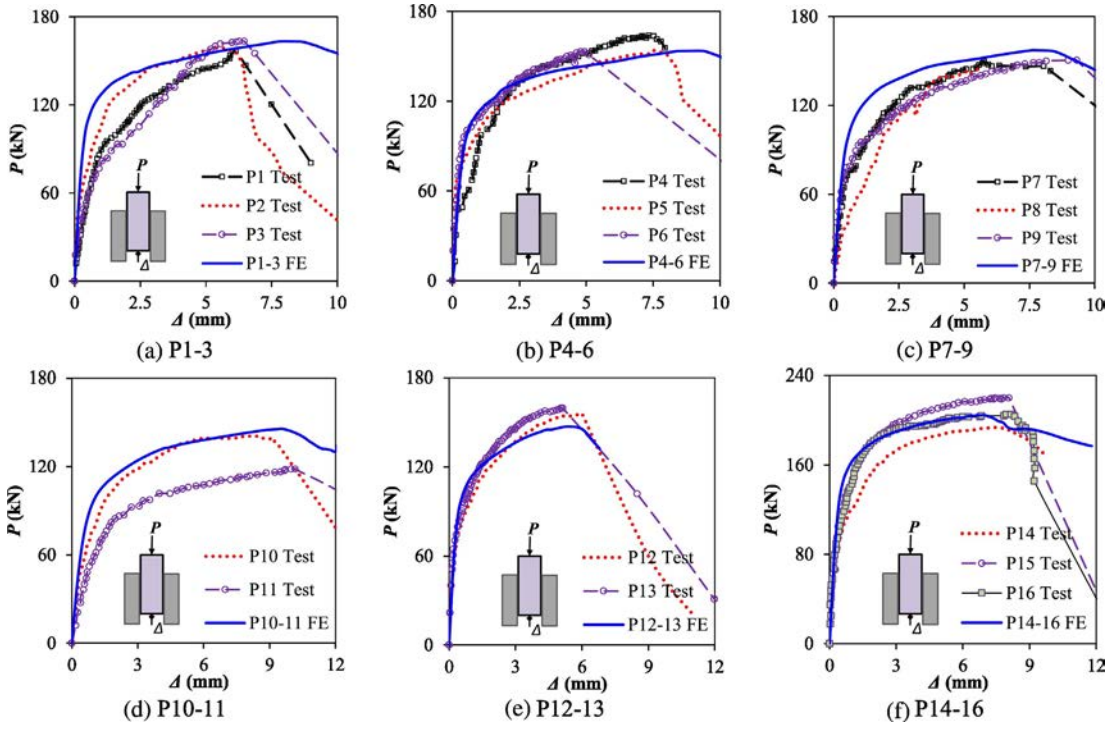

Fig. 8. Comparisons of the load-slip curves for push-out tests between FE predictions and tests.

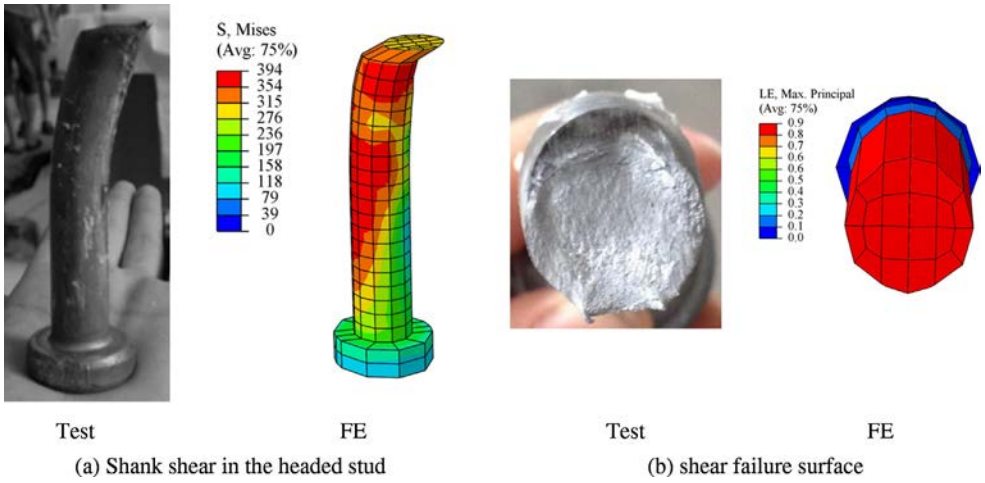

Fig. 9. Comparisons of shear failure in the connectors between FE simulation and tests.

4.2. Validations of the FE model against steel-elastic concrete composite beam tests

Fig. 10 compares the FE predicted load-central deflection curves with the experimental curves of the steel-elastic concrete composite beams. It can be seen that the FE predicted load-central deflection curves resemble well with the experimental results especially in terms of elastic stiffness, ultimate resistance, and the plastic behaviours. Table 3 also compares the FE predicted elastic stiffness of the load-central deflection curves and ultimate resistances with those experimental values. It can be found that the FE model averagely overestimates the elastic stiffness of the steel-elastic composite beam by 1% with a standard deviation (Stdev) of 9% and averagely underestimates the ultimate resistance by 1% with a Stdev of only 3% for the six specimens. These comparisons implied that the developed FE model offered reasonable estimations on the deforming behaviours and ultimate resistances with slight errors of about 1%.

Fig. 11 compares the experimental load-end slip (relative slip between the concrete slab and I-beam at the end of the beam) behaviours of the steel-elastic concrete composite beams with those FE predicted curves. It can be observed that the FE predicted load versus end slip curves resemble reasonably well with the measured curves during the test even though there were slight differences. The differences between the FE predicted and experimental load-end slip curves may be due to the initial bonding between the I-beam and concrete slabs. However, this bonding tends to be complex that depends on the imperfections of the I-beam, concrete-steel bonding, and relative stiffness between the steel and concrete, which is difficult to simulate.

Fig. 12 compares the experimental failure modes with the FE simulations. It can be found that the developed FE model could predict well

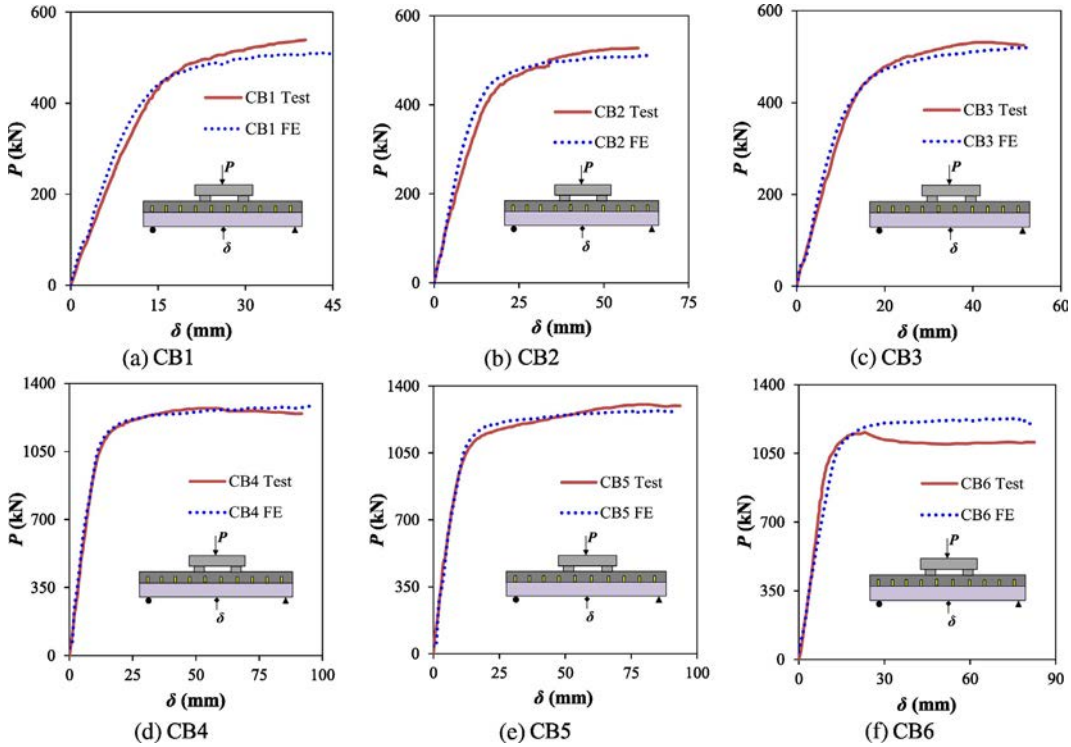

Fig. 10. Comparisons of the FE predicted load-central deflections with the experimental curves of the steel-elastic concrete beams.

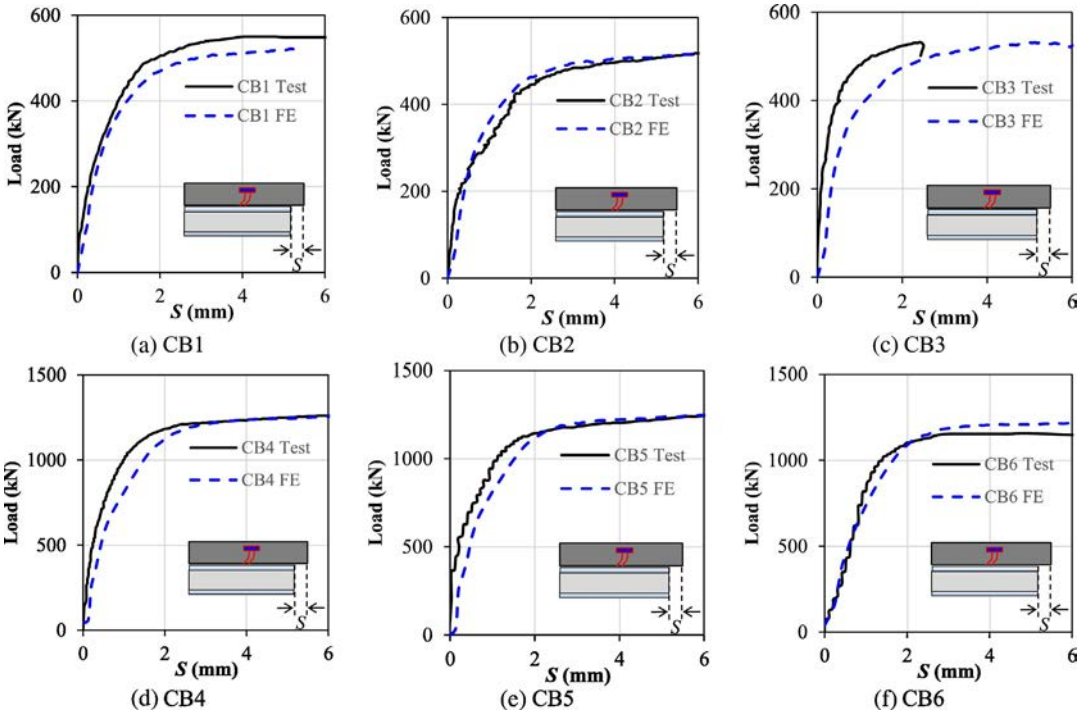

Fig. 11. Comparisons of load-end slip curves in beams between tests and FE simulation.

the local buckling in the flange of the I-beam and the cracks developed in the concrete slabs.

These comparisons confirmed that the developed FEM could offer exact simulations on the ultimate strength behaviour of the steel-elastic concrete beams in terms of load-deflection curves, ultimate resistances, relative slip behaviour between the concrete slabs and I-beam, and failure modes.

From the above validations of the FE model against push-out tests and steel-elastic concrete composite beam tests, it can be found that the developed FE model could offer reasonable simulation on the ultimate strength behaviour of steel-elastic concrete structure from the basic component level (i.e., single connector) to the structural level (i.e., steel-elastic concrete composite beams).

4.3. Parametric study

4.3.1. Descriptions of the cases in the parametric study

With the validated FE model, a parametric study was carried out. The geometry and dimension of the specimens follows the details of the representative beams CB1 and CB3 that were used for the validations of the

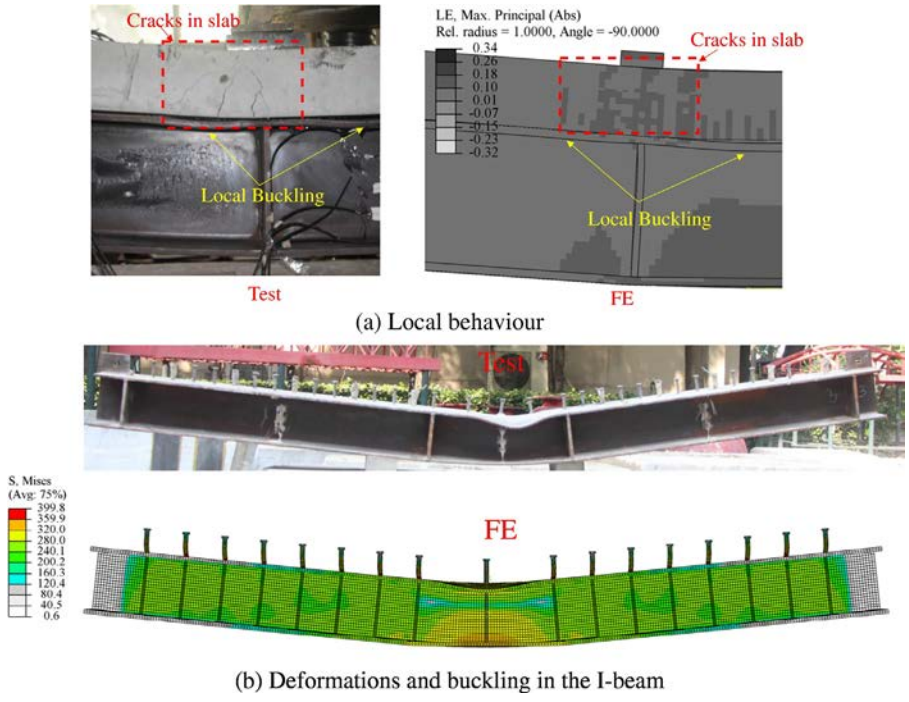

Fig. 12. Comparisons of failure mode between FE simulations and tests in SECC beam.

Table 4
Mix proportions of different elastic concretes (kg/m^3).

Type	Rubber (%)	OPC (kg)	Fly ash (kg)	Mineral Powder (kg)	CA (kg)	FA (kg)	SP (kg)
EC1-0%	0	353	113	0	1301	434	0
EC2-5%	5	339	113	57	1155	385	5.1
EC3-8%	8	339	170	0	1095	365	5.5
EC4-10%	10	339	113	57	1051	350	5.1
EC5-12%	12	339	113	57	1011	337	5.1
EC5-15%	15	339	113	57	964	321	5.1

OPC denotes ordinary Portland cement; CA denotes granite type of coarse aggregate; FA denote natural sand type of fine aggregate; SP denotes the superplasticizer.

FE model. The details of CB1 and CB3 are given in Table 3 and Fig. 3. The parameters chosen in the FE parametric study are as the follows;

(a) Volume fraction of the fiber content ρ (%). Different volume fractions of fiber content were chosen in the parametric study, i.e., $\rho = 0\%$, 5%, 8%, 10%, 12%, and 15%. The concrete mix proportions for these elastic concrete with different volume content of crumb rubber are listed in Table 4.
(b) Strength of the I-beam. Grade S275, S355, S460, and S690 steels were selected for the I-beam to investigate the strengths of the I-beam on the ultimate strength behaviour of the steel-elastic concrete composite beam.

Table 5 lists the details of all the cases in this parametric study.

4.3.2. Effect of volume fractions of the rubber in the elastic concrete on ultimate resistance

Fig. 13 depicts the load-central deflection curves of the FE analysis cases of SECC beams with the volume fraction of the rubber ρ. It can be seen that as the volume fraction of the rubber ρ increases from 0 to 15%, its influence on the ultimate resistance of the SECC composite beams is quite limited. This observation was consistent with the experimental observations reported by Han et al. [10]. Though the compressive strength and elastic modulus of the elastic concrete decreased as ρ increases, the ultimate resistance of the SECC beam was not weakened. According to the specifications in Eurocode 4 [37] and ACI 318 [38], the shear resistance of the headed studs decreases with the decrease of the compressive strength and elastic modulus of the concrete. However, these specifications in the design codes were derived from the regression analysis on the push-out tests and they still own limitations. Fig. 4 shows that elastic concrete behaves differently from the typical normal weight (or lightweight) concrete in terms of the compressive and tensile stress-strain curves. Moreover, the push-out tests reported by Han et al. [10] also showed that, for the push-out tests with 10% of rubber, even though the strength and elastic modulus of the elastic concrete was decreased, the shear resistances of the connectors were only decreased by 6% and the failure mode was still shank shear mode. This might explain the limited influence of the rubber content of the elastic concrete on the ultimate load carrying capacity of the SECC beams.

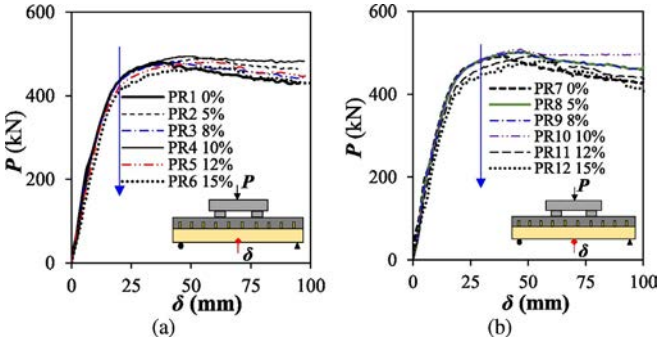

Fig. 13. Effect of rubber content on ultimate strength behaviour of SECC beam.

This observation further confirmed the advantage of the applications of the elastic concrete in the steel-concrete composite structures, and the ultimate load carrying capacity of the steel-concrete composite beams were not compromised by introducing the elastic concrete with different rubber content.

4.3.3. Effect of different strengths of the steel used for the I-beam

High strength steel becomes popular in the engineering constructions with advantages of significantly improved yield strength but slight increase in the costs. Fig. 14(a)–(c) shows the effect of different high strength of steel I-beam on the ultimate load carrying capacities of the SECC beams. It can be observed that the ultimate resistance of the SECC beams was significantly increased by introducing high strength steel in the SECC beams. As the yield strength of the steel in I-beam increased from 275 MPa to 355 MPa, 460 MPa, and 690 MPa, the ultimate resistances for SECC beams with 0%, 5%, and 10% rubber content were all increased by 21%, 46%, and 94%, respectively. Meanwhile, these

Table 5
Details and results of different cases in FE parametric studies.

Specimen	Prototype	$S1$ (mm)	ρ (%)	f_c (MPa)	E_c (GPa)	f_y (MPa)	f_u (MPa)	E_s (GPa)	σ_y (MPa)	σ_u (MPa)	n_s	λ	P_u (kN)
PR1	CB1	140	0	35.5	30.2	275	430	205	360	505	16.5	0.51	480
PR2	CB1	140	5	35.8	20.7	275	430	205	360	505	16.5	0.43	491
PR3	CB1	140	8	33.1	18.8	275	430	205	360	505	16.5	0.39	481
PR4	CB1	140	10	30.6	15.1	275	430	205	360	505	16.5	0.35	495
PR5	CB1	140	12	28.2	9.98	275	430	205	360	505	16.5	0.30	482
PR6	CB1	140	15	21.0	5.72	275	430	205	360	505	16.5	0.26	469
PR7	CB3	100	0	35.5	30.2	275	430	205	360	505	12.5	0.39	495
PR8	CB3	100	5	35.8	20.7	275	430	205	360	505	12.5	0.32	501
PR9	CB3	100	8	33.1	18.8	275	430	205	360	505	12.5	0.30	502
PR10	CB3	100	10	30.6	15.1	275	430	205	360	505	12.5	0.26	509
PR11	CB3	100	12	28.2	9.98	275	430	205	360	505	12.5	0.22	496
PR12	CB3	100	15	21.0	5.72	275	430	205	360	505	12.5	0.20	481
PR13	CB1	140	0	35.5	30.2	355	490	210	360	505	16.5	0.46	581
PR14	CB1	140	0	35.5	30.2	460	560	210	360	505	16.5	0.46	702
PR15	CB1	140	0	35.5	30.2	690	725	210	360	505	16.5	0.46	931
PR16	CB1	140	5	35.8	20.7	355	490	210	360	505	16.5	0.38	594
PR17	CB1	140	5	35.8	20.7	460	560	210	360	505	16.5	0.38	718
PR18	CB1	140	5	35.8	20.7	690	725	210	360	505	16.5	0.38	954
PR19	CB1	140	10	30.6	15.1	355	490	210	360	505	16.5	0.35	603
PR20	CB1	140	10	30.6	15.1	460	560	210	360	505	16.5	0.35	724
PR21	CB1	140	10	30.6	15.1	690	725	210	360	505	16.5	0.35	964

f_c, E_c denote compressive strength and elastic modulus of concrete, respectively; λ denotes composite action.

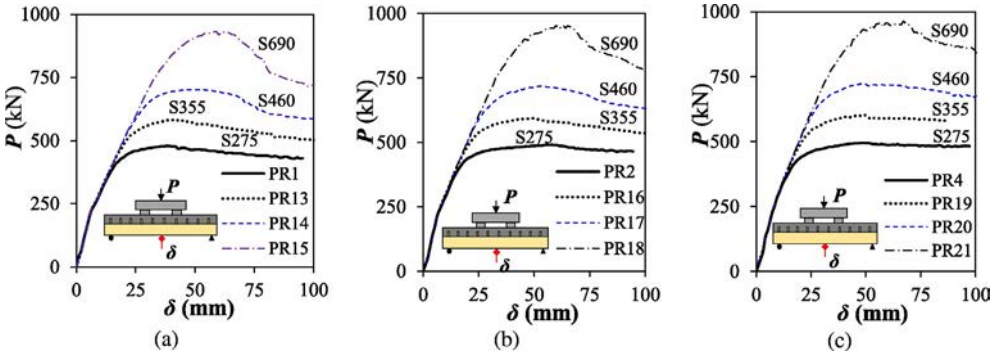

Fig. 14. Effect of strength of the steel for I-beam on ultimate strength behaviour of SECC beam.

increments for SECC beam with 0% and 5% rubber content are about 22%, 46%, and 95%, respectively. In addition, all the SECC beams with different strength steels failed in ductile flexure mode. These observations implied that using the high strength steel maybe an economic and effective solution to increase the ultimate loading carrying capacity of the SECC beams.

5. Recommended finite element analysis procedures for SECC structures

Based on the developments of the FE modelling, extensive validations, and parametric studies, the recommended FE analysis procedures were given for the SECC structures;

(a) Obtaining the basic mechanical properties of the elastic concrete with different rubber content through compressive and tensile tests on the elastic concrete cylinders or prisms.
(b) Modelling the I-beam with geometry and materials as used in the tests.
(c) Modelling the headed studs with the specified spacing and geometry in the specimens.
(d) Modelling the concrete slabs with the same materials and reserving the holes for the headed studs used in the SECC beams.
(e) Modelling the reinforcement mesh used in the concrete slabs.
(f) Defining the interactions among different interacting pairs in the SECC beam, e.g., interaction pair between I beam and concrete slab, interaction between headed stud and concrete slab, interaction between support and I-beam, and interaction between loading platen and concrete slab.
(g) Running the analysis and making sure the convergence of solutions.

6. Conclusions

This paper firstly summarized the experimental studies on the steel-elastic concrete composite (SECC) structures. A finite element model (FEM) for the SECC structure has been developed that offered detailed simulation on the headed stud connectors and considered nonlinearities of both steel and elastic concrete materials. The accuracy of the developed FEM was extensively checked by 16 push-out tests and six full scale beam tests that all adopted elastic concrete in the concrete slabs. With the validated FEM, a parametric study consisting of 21 cases was carried out to investigate the influences of the rubber content in elastic concrete and strength of the I-beam on the ultimate load carrying capacity of the SECC beams. Based on these numerical studies, the following observations and conclusions are drawn;

(1) The validations of the FE analyses against 16 push-out tests proved that the developed FEM offered reasonably accurate simulations on the ultimate strength behaviours of the SECC structures at the component level. The FEM averagely underestimated the shear resistance of the headed studs in the elastic concrete by 2% with COV of 7% for 16 push-out tests.
(2) Through validations against six tests on SECC beams, it was proved that the developed FEM could accurately simulate the ultimate strength behaviour of the SECC structures at the structural level in terms of load-deflection behaviours, ultimate resistances, failure modes, and slip at steel-concrete interface. The average and COV for the test-to-prediction ratios of the six tests were 1.01 and 0.03, respectively.
(3) The parametric study using the validated FEM showed that adding 0– 15% rubber (by volume) to the elastic concrete did not weaken the ultimate strength behaviour of the SECC beam in terms of load-deflection behaviours and ultimate resistances. This may prove the advantages of the SECC beams.
(4) The FE parametric study showed that increasing the yield strength of the I-beam from 275 MPa to 355 MPa, 460 MPa, and 690 MPa leads to the increments in the ultimate resistances of the SECC beams of 22%, 46%, and 95%, respectively. Thus, introducing I-beams with high strength steel may be a quite economic and effective way to improve the ultimate strength behaviour of the SECC beams.
(5) Based on the FE modelling and validations, step-by-step FE analysis procedures were recommended for the nonlinear numerical analysis on the SECC beams.

Acknowledgements

The authors would like to thank Prof. Qinghua Han and Dr. Jie Xu for providing the experimental results.

References

[1] N.N. Eldin, A.B. Senouci, Rubber-tire particles as concrete aggregate, J. Mater. Civ. Eng. 5 (4) (1993) 478–496.
[2] N.N. Eldin, A.B. Senouci, Measurement and prediction of the strength of rubberized concrete, Cem. Concr. Compos. 16 (4) (1994) 287–298.
[3] I.B. Topçu, The properties of rubberized concretes, Cem. Concr. Res. 25 (2) (1995) 304–310.
[4] H.A. Toutanji, The use of rubber tire particles in concrete to replace mineral aggregates, Cem. Concr. Compos. 18 (2) (1996) 135–139.
[5] A. Turatsinze, M. Garros, On the modulus of elasticity and strain capacity of self-compacting concrete incorporating rubber aggregates, Resour. Conserv. Recycl. 52 (10) (2008) 1209–1215.
[6] E. Ganjian, M. Khorami, And a.A.Maghsoudi AA. Scrap-Tyre-rubber replacement for aggregate and filler in concrete, Constr. Build. Mater. 23 (5) (2009) 1828–1836.
[7] W.X. Feng, F. Liu, W.H. Zheng, Test of fatigue performance of rubberized concrete, J. Build. Mater. 15 (4) (2012) 469–473.
[8] S.H. Kim, C.Y. Jung, J.H. Ahn, Ultimate strength of composite structure with different degrees of shear connection, Steel Compos. Struct. 11 (5) (2011) 375–390.
[9] J.G. Nie, J.S. Fan, C.S. Cai, Experimental study of partially shear-connected composite beams with profiled sheeting, Eng. Struct. 30 (1) (2008) 1–12.
[10] Q.H. Han, J. Xu, Y. Xing, Z.L. Li, Static push-out test on steel and recycled tire rubber-filled concrete composite beams, Steel Compos. Struct. 19 (4) (2015) 843–860.
[11] Y. Xing, Q.H. Han, J. Xu, Q. Guo, Y. Wang, Experimental and numerical study on static behavior of elastic concrete-steel composite beams, J. Constr. Steel Res. 123 (2016) 79–92.

[12] Q.H. Han, Y. Wang, J. Xu, Numerical analysis on shear stud in push-out test with crumb rubber concrete, J. Constr. Steel Res. 130 (2017) 148–158.
[13] Q.H. Han, Y.H. Wang, J. Xu, Y. Xing, Fatigue behavior of stud shear connectors in steel and recycled type rubber-filled concrete composite beams, Steel Compos. Struct. 22 (2) (2016) 353–368.
[14] I.M. Viest, Investigation of stud shear connectors for composite concrete and steel T-beams, ACI 52 (4) (1957) 875–892.
[15] J.G. Ollgaard, R.G. Slutter, J.W. Fisher, Shear strength of stud connectors in lightweight and normal-weight concrete, AISC Eng. J. 8 (2) (1971) 55–64.
[16] D. Lam, Capacities of headed stud shear connectors in composite steel beams with precast hollow core slabs, J. Constr. Steel Res. 63 (2007) 1160–1174.
[17] M.M. Tahir, P.N. Shek, C.S. Tan, Push-off tests on pin-connected shear studs with composite steel-concrete beams, Constr. Build. Mater. 23 (9) (2009) 3024–3033.
[18] J.B. Yan, J.Y.R. Liew, K.M.A. Sohel, M.H. Zhang, Push-out tests on J-hook connectors in steel–concrete–steel sandwich structure, Mater. Struct. 47 (10) (2014) 1693–1714.
[19] M. Xie, N. Foundoukos, J.C. Chapman, Experimental and numerical investigation on the shear behaviour of friction-welded bar–plate connections embedded in concrete, J. Constr. Steel Res. 61 (2004) 625–649.
[20] H.T. Nguyen, S.E. Seung Eock Kim, Finite element modeling of push-out tests for large stud shear connectors, J. Constr. Steel Res. 65 (10–11) (2009) 1909–1920.
[21] M. Pavlović, Z. Marković, M. Veljković, D. Buđevac, Bolted shear connectors vs. headed studs behaviour in push-out tests, J. Constr. Steel Res. 88 (2013) 134–149.
[22] D. Lam, E. El-Lobody, Finite element modelling of headed stud shear connectors in steel-concrete composite beam, Structural Engineering, Mechanics and Computation, 1, 2001, pp. 401–408.
[23] S. Guezouli, A. Lachal, Q.H. Nguyen, Numerical investigation of internal force transfer mechanism in push-out tests, Eng. Struct. 52 (2013) 140–152.
[24] K.M.A. Sohel, J.Y.R. Liew, C.G. Koh, Numerical modelling of lightweight steel-concrete-steel sandwich composite beams subjected to impact, Thin-Walled Struct. 94 (2015) 135–146.
[25] G.Z. Zhao, A. Li, Numerical study of a bonded steel and concrete composite beam, Comput. Struct. 86 (19–20) (2008) 1830–1838.
[26] T.Y. Song, L.H. Han, Post-fire behaviour of concrete-filled steel tubular column to axially and rotationally restrained steel beam joint, Fire Saf. J. 69 (2014) 147–163.
[27] J.B. Yan, Finite element analysis on ultimate strength behaviour of steel-concrete-steel sandwich composite beam structures, Mater. Struct. 48 (6) (2015) 1645–1667.
[28] GB/T50081-2002. Chinese Industrial Standard of Building Material, GB/T50081-2002, Test Methods of Mechanics Property of Ordinary Concrete, 2002.
[29] Chinese Industrial Standard of Building Material, T0555-2005, Test Method of Prismatic Compressive Strength of Cement Concrete, 2005.
[30] ASTM A 370-13, Standard Test Methods and Definitions for Mechanical Testing of Steel Products, ASTM International, 100 Barr Harbor Drive, PO Box C700, West Conshohocken, PA 19428-2949, United States, 2013.
[31] Q.H. Han, Y.H. Wang, J. Xu, Y. Xing, Static behaviour of stud shear connectors in elastic concrete-steel composite beams, J. Constr. Steel Res. 113 (2015) 115–126.
[32] ABAQUS, ABAQUS Standard User's Manual, Version 6.12, Dassault Systemes Corp., Providence, RI (USA), 2012.
[33] J. Lee, G.L. Fenves, Plastic-damage model for cyclic loading of concrete structures, J. Eng. Mech. 124 (8) (1998) 892–900.
[34] D. Carreira, K. Chu, Stress-strain relationship for plain concrete in compression, J. ACI Struct. 82 (11) (1985) 797–804.
[35] H. Zhu, C.S. Liu, Y.M. Zhang, Z.G. Li, Effect of crumb rubber proportion on compressive and flexural behavior of concrete, J. Tianjin Univ. 40 (7) (2007) 761–765.
[36] J.C. Wang, Y.K. Chen, Applications of ABAQUS in Civil Engineering (in Chinese), Press of Zhejiang University, Publication No. C2118999F, China, 2006.
[37] Eurocode 4, Design of Composite Steel and Concrete Structures-Part 1.1: General Rules and Rules for Buildings, BS EN 1994-1-1, 2004.
[38] American Concrete Institute 318 (ACI), Building Code Requirements for Structural Concrete (ACI 318–11) and Commentary, American Concrete Institute, Farmington Hills (MI), 2011.